



Published in final edited form as:

*J Am Chem Soc.* 2013 April 10; 135(14): 5312–5315. doi:10.1021/ja401555y.

## Nickel(II) Dithiocarbamate Complexes Containing Sulforhodamine B as Fluorescent Probes for Selective Detection of Nitrogen Dioxide

Yan Yan<sup>†</sup>, Saarangan Krishnakumar<sup>†</sup>, Huan Yu<sup>‡</sup>, Srinivas Ramishetti<sup>§</sup>, Lih Wen Deng<sup>||</sup>, Suhua Wang<sup>\*‡</sup>, Leaf Huang<sup>§</sup>, and Dejian Huang<sup>\*†</sup>

<sup>†</sup>Department of Chemistry, National University of Singapore, 3 Science Drive 3, Singapore 117543, Singapore

<sup>‡</sup>Institute of Intelligent Machines, Chinese Academy of Sciences, Hefei, Anhui, 230031, China

<sup>||</sup>Department of Biochemistry, Yong Loo Lin School of Medicine, National University of Singapore, National University Health System, 8 Medical Drive, Singapore 117597, Singapore

<sup>§</sup>Division of Molecular Pharmaceutics, Eshelman School of Pharmacy, University of North Carolina at Chapel Hill, Chapel Hill, NC 27599, USA.

### Abstract

We synthesized the Ni(II) complexes with dithiocarbamate ligand derived from *ortho* and *para* isomers sulforhodamine B fluorophores and demonstrated they are highly selective in reaction with nitrogen dioxide (NO<sub>2</sub>). Comparing to the *para* isomer, the *ortho* isomer showed much greater fluorescence increase upon reaction with nitrogen dioxide, which led to oxidation and de-complexation of dithiocarbamate ligand from Ni(II). We applied this probe for visual detection of 1 ppm nitrogen dioxide in gas phase and fluorescence imaging of NO<sub>2</sub> in macrophage cells treated with nitrogen oxide donor.

As a dominant component in the NO<sub>x</sub> (x = 1 or 2) family, nitrogen dioxide (NO<sub>2</sub>) is a major air pollutant generated from high temperature oxidation of molecular nitrogen by oxygen in combustion.<sup>1</sup> Whereas biologically, nitrogen dioxide is implicated as the root cause of toxic effects of reactive nitrogen species derived from nitric oxide oxidation by oxygen in the cellular system<sup>2</sup> and from one-electron reduction of nitrite by metalloenzymes.<sup>3</sup> As an air stable and strong lipophilic oxidant, nitrogen dioxide can trigger lipid auto-oxidation<sup>4</sup> and oxidative nitration of aromatic amino acids, particularly tyrosine.<sup>5</sup> However, there is a lack of selective fluorescent probes for convenient detection of nitrogen dioxide. Most fluorescent probes reported are for nitric oxide (NO) detection. While transition metal complex based probes contain the nitric oxide reactive metal as fluorescence quencher,<sup>6-10</sup> the organic dye based probes detect nitric oxide indirectly through oxidation of aromatic

\*Corresponding Authors Dejian Huang, chmhdj@nus.edu.sg Suhua Wang, shwang@iim.ac.cn.

Supporting Information Synthetic procedures and spectroscopic data of compounds **1** to **6**, crystal structure of **1** and **2**, and experimental procedures of cell imaging and selectivity of the probe towards different ROS. These material is available free of charge via the Internet at <http://pubs.acs.org>.

amines by  $\text{N}_2\text{O}_3$ ,<sup>11-12</sup>, which is produced via oxidation of NO by  $\text{O}_2$ .<sup>13-14</sup> We herein report the first fluorescent probe for selective detection of nitrogen dioxide, containing Ni(II) as a fluorescence quencher and  $\text{NO}_2$  reaction center.

Reaction of sulforhodamine with oxalyl chloride yielded a mixture of two isomeric compounds with  $-\text{SO}_2\text{Cl}$  group in *para* or *ortho* position of the phenyl ring.<sup>15</sup> The mixture was treated directly with piperazine and two isomers produced were separated readily by column chromatography to give *para* isomer, **1** and *ortho* isomer, **2** (Scheme 1). Due to their similarity, it was difficult to unambiguously distinguish their structures based on NMR and MS spectra alone. Hence the structures of the isomers were determined by single crystal X-ray diffractions (Figure S1) and, accordingly, the  $^1\text{H}$  NMR spectral data was assigned with certainty. In the presence of sodium hydroxide, the two isomers reacted readily with carbon disulfide to produce dithiocarbamate sodium salts **3** and **4**, respectively. Dithiocarbamate is a bidentate ligand that promptly forms complexes with many transition metals, leading to quenching of the ligand fluorescence. It is reported that Ni(II) bisdithiocarbamate complexes,  $\text{Ni(II)(RNCS}_2)_2$ , reacts immediately with nitrogen dioxide to yield the oxidative dimerized ligand,  $(\text{RNCS}_2)_2$ ,<sup>16</sup> which could be fluorescent if R is a fluorophore. Hence, in order to prepare a Ni(II) based turn-on fluorescent probe for nitrogen dioxide, we mixed nickel(II) nitrate with **3** and **4** at 1 to 2 ratio and prepared **5** and **6** (Scheme 1). The structures of **5** and **6** were characterized by  $^1\text{H}$  NMR and the results were in agreement with a diamagnetic nickel complex with square-planar configuration. Additionally, their MALDI-TOF mass spectra showed isotope distribution pattern matching the expected molecular formula (Figure S2).

To illustrate the effect of two isomers on fluorescence quenching, the fluorescence quantum yields of compounds shown in Scheme 1 were measured (Table S1). The presence of piperazine group at *ortho* position (**2**, QY = 0.21) has reduced the quantum yield of the parent compound (sulforhodamine B, QY = 0.34) more significantly than the *para* isomer (**1**, QY = 0.28). Dithiocarbamate groups further reduced the quantum yield a little bit. The *ortho* isomer of the Ni(II) complex has the lowest quantum yield, and is 70 times lower than the ligand itself, while the *para* isomer **5** has only five times lower quantum yield comparing to **3**. Energy transfer is not likely due to the small absorbance bands overlap between fluorophore emission and quencher absorption (Figure S3).

The mechanism behind fluorescence quenching is probably attributed to photo-induced electron transfer (PeT) from electron donor Ni(II) to sulforhodamine B excited state. The HOMO and LUMO energies of  $\text{Ni(Me}_2\text{NCS}_2)_2$  was calculated to be  $-4.09$  and  $-1.03$  eV respectively and dithiocarbamate ligand is known to stabilize Ni(III).<sup>17</sup> Whereas the HOMO and LUMO of rhodamine B was  $-8.058$  and  $-5.266$  eV respectively.<sup>18</sup> Therefore, PeT from Ni to rhodamine B chromophore is energetically favored. PeT is highly sensitive to the distance between the fluorophore and the quencher; therefore, the shorter distance of Ni to the center of the fluorophore in **6** is likely to cause a much higher quenching efficiency than **5**. From the crystal structures of **1** and **2**, the distances of nitrogen (NH) in piperazine group to the centers of the fluorophore were calculated to be  $9.4$  and  $7.4$  Å, respectively. Although we failed to obtain single crystal structures of the Ni complexes, it is reasonable to assume that the distance of the Ni to the rhodamine B chromophore would be shorter in **6** in

comparison to that in **5**. It should be born in mind that in solution, molecular motions will have significant effect on the distances.

We evaluated the selectivity of the *ortho* isomer **6** towards common reactive oxygen species (ROS) in methanol (Figure S5). Only NO<sub>2</sub> could increase the fluorescence intensity by more than 12 times, whereas other biological relevant ROS could not do so. Neither nitrite nor nitrate could switch on the fluorescence. Moreover, addition of nitric oxide donor diethylamine NONOate (DEANO) rapidly turned on the fluorescence by 12 fold within minutes and there was excellent dose response between the fluorescence intensity and the DEANO concentrations (Figure S7). In comparison, when *para* isomer **5** is used, the magnitude of fluorescence increase is only 1.9 times (Figure S6). Although there is a sulfonate group on the fluorophore of probe **6**, its water solubility is extremely poor. In aqueous media (water and buffer), there was no fluorescence intensity gain after addition of NO<sub>2</sub>. It turned out that the reaction products precipitated out even at micromolar concentration level used in the experiment. Addition of surfactant (Tween 20) to the reaction mixture before adding NO<sub>2</sub> led to fluorescence turning on. Therefore, to introduce the probe into physiological condition, we applied DOTAP (1,2-dioleoyl-3-trimethylammonium-propane chloride salt) liposome as a delivery vehicle for our probe. It is found that probe **6** delivered by DOTAP demonstrated excellent selectivity to NO<sub>2</sub> (Figure 1) and good dose-response to DEANO (Figure 2) in buffered aqueous media to simulate the physiological conditions.

To further test whether the probe is sensitive to nitric oxide or nitrogen dioxide, we carried out the reaction in the absence of oxygen by degassing the probe solutions and DEANO solutions before mixing them under nitrogen, and we failed to observe any fluorescence turning-on event. This observation showed that the fluorescence turning-on by DEANO required oxygen, suggesting that it is NO<sub>2</sub> that reacts with the probe as NO generated from DEANO is rapidly oxidized to NO<sub>2</sub> by oxygen present in the solution.<sup>19</sup> This was confirmed by a separate test in which the response of the probe to NO<sub>2</sub> gas formed by mixing NO and air or commercial NO<sub>2</sub> gas was examined. Indeed, fluorescence was turned on. To further verify if the reaction products of **6** with DEANO in the presence of air and with NO<sub>2</sub> gas are identical, the reaction products were analyzed using HPLC and LC-MS. The results suggested that the same major products with fluorescence were generated by the probe reacted with DEANO in the presence of air and with NO<sub>2</sub> gas in methanol. These results clearly show that NO<sub>2</sub> can turn on the fluorescence of the probe. Moreover, the *para* isomer **5** also reacted with NO<sub>2</sub> in the same way as the *ortho* isomer **6**, as characterized by HPLC chromatograms (Figure 3).

The structures of the reaction products were then deduced on the basis of LC-MS<sup>n</sup> spectra and shown in Scheme 2. Apparently, NO<sub>2</sub> brought forth the oxidation of dithiocarbamate ligand and generated Ni(II) free compounds with high fluorescence. We proposed that the reaction is initiated by NO<sub>2</sub> adduct with **5/6**, forming Ni(III)(R<sub>2</sub>NCS<sub>2</sub>)<sub>2</sub>(NO<sub>2</sub>). Subsequent intramolecular electron transfer reaction forms Ni(II) complex and R<sub>2</sub>NCS<sub>2</sub>• radical, which couples to give ligand dimer shown in peak **B/B'** (Scheme 2). The compound shown in peak **A/A'** is generated due to secondary oxidation reaction of (R<sub>2</sub>NCS<sub>2</sub>)<sub>2</sub> followed by methanolysis. Consistent with the two proposed compounds, ESI-MS results of the

compound shown in peak **A/A'** gave  $[M+H]^+$  peak at  $m/z = 749.2$  and  $[M+Na]^+$  peak at  $m/z = 771.2$ , while ESI-MS results of compound for **B/B'** demonstrated two dications,  $[M+2H]^{2+}$  at  $m/z = 702.2$  and  $[M+2Na]^{2+}$  at  $m/z = 724.2$ , respectively. Our assignments are supported by ESI-MS<sup>2</sup> fragmentation patterns of **A'/B'**. MS<sup>2</sup> spectrum of peak **A'** shown three fragments at 717.1 ( $(M+H)^+ - CH_3OH$ ), 669.2 ( $(M+H)^+ - SO_3$ ), and 637.0 ( $(M+H)^+ - CH_3OH - SO_3$ ), respectively. MS<sup>2</sup> spectrum of **B'** gave a peak at  $m/z = 627.2$  formed from the molecular cation through homolytic cleavage of the S-S bond followed by losing a CS<sub>2</sub> (Figure S4).

In addition, the formula of **A'** and **B'** were confirmed by high resolution MS spectra (Table S2). Our results are in agreement with literature work, which showed that bis(diethyldithiocarbamate)nickel(II) (Ni(dtc)<sub>2</sub>) reacted with NO<sub>2</sub>, but not with NO, to give corresponding paramagnetic Ni(III)(dtc)<sub>3</sub> as an intermediate, which decomposed to oxidized dithiocarbamate ligand, i.e. thiuram disulfide ((R<sub>2</sub>NCS<sub>2</sub>)<sub>2</sub>).<sup>16</sup>

Considering the high toxicity of NO<sub>2</sub> in atmosphere, Health and Safety Commission (HSC) of USA has approved Occupational Exposure Standards (OESs) of 1 ppm (8-hour time weighted average) and 5 ppm (short-term exposure limit) for NO<sub>2</sub>.<sup>20</sup> Convenient detection of gaseous NO<sub>2</sub> would be ideal for monitoring air pollution due to NO<sub>x</sub> (x = 1 or 2, with NO<sub>2</sub> being dominant species). For this purpose, probe **6** was successfully applied in visual detection of gaseous NO<sub>2</sub> with the detection limit reaching 1.0 ppm using NO<sub>2</sub> indicator strips prepared by dropping methanol/chloroform (1:1) solution of **6** (800 nM) on filter paper to give round stains of *ca.* 5 mm in diameter after solvent evaporation. The NO<sub>2</sub> indicator strips were exposed to different concentrations of NO<sub>2</sub> gas for 10 minutes. Under regular laboratory lighting conditions, there was no apparent spot detected for all indicator strips (Figure 4 right). When the strips were exposed to UV lamp (352 nm), red fluorescence spots could be observed visually for strips exposed to NO<sub>2</sub> gas at concentration as low as 1.0 ppm and the fluorescence intensity increased in a dose dependent manner at 10 and 100 ppm NO<sub>2</sub> (Figure 4 left). The results demonstrated that this NO<sub>2</sub> indicator strips immobilized with probe **6** is a simple, direct and economical tool for rapid detection of gaseous NO<sub>2</sub> at low concentrations.

To introduce the probe into biological system, liposomal carrier was applied. Cationic liposomes have been studied extensively in gene therapy applications and also cationic lipids are effective in vaccine formulations to treat cancers.<sup>21-22</sup> Therefore, we applied DOTAP liposome as a delivery vehicle for our probe. Although it is known that DOTAP liposome at high concentration is toxic to cells, our observation showed that RAW 264.7 cells can withstand up to 100 μM DOTAP (Figure S8). To illustrate that the probe **6** uptake by cells can be turned on by adding NO<sub>2</sub>, the RAW 264.7 cells treated with DOTAP liposome containing **6** (5 μM) were further treated with DEANO as a NO<sub>2</sub> donor.<sup>19</sup> The fluorescence images of the cells (Figure 5B, D) clearly illustrate that fluorescence intensity could be efficiently enhanced by adding DEANO (for intensity plot please refer to Figure S9). Moreover, the Z-stack gallery image (Figure S10) clearly shows that RAW 264.7 cells were able to efficiently uptake the probe **6** dispersed in DOTAP. A 3D image (Figure 5A, B, C, D) was also given to demonstrate the depth distribution of probe **6** inside cells, both treated and not treated with DEANO.

In conclusion, we have demonstrated that dithiocarbamate Ni(II) complexes containing sulforhodamine B fluorophore is a highly selective probe for detection of nitrogen dioxide. To the best of our knowledge, this is the first example of live cell fluorescence imaging of NO<sub>2</sub> activity and visual detection of gaseous NO<sub>2</sub> at low concentrations. Many third row transition metals are good fluorescence quenchers because their complexes with fluorescent ligands are paramagnetic due to the unpaired metal d electrons. In contrast, Ni(II) coordination sphere in complex **5** and **6** adopt square planar geometry and are diamagnetic. It warrants further research on understanding the quenching mechanisms of Ni(II) and developing even more sensitive probes with rationale combination of fluorophore and nickel complex.

## Supplementary Material

Refer to Web version on PubMed Central for supplementary material.

## Acknowledgments

DH and LWD thank the Agency of Science, Technology and Research (A \*Star) of Singapore for financial support (grant number: 112 177 0036). DH and SW thank the National Natural Science Foundation of China for a grant (grant number: 21228702). LH thanks the National Institute of Health for a grant (number: CA129421).

## REFERENCES

1. Bascom R, P A, Costa DA, Devlin R, Dockery DW, Frampton MW, Lambert W, Samet JM, Speizer FE, Utell M. *Am. J. Respir. Crit. Care Med.* 1996; 153:3–50. [PubMed: 8542133]
2. Lewis RS, Tamir S, Tannenbaum SR, Deen WM. *J. Biol. Chem.* 1995; 270:29350–29355. [PubMed: 7493969]
3. Bian K, Gao Z, Weisbrodt N, Murad F. *Proc. Natl. Acad. Sci. USA.* 2003; 100:5712–5717. [PubMed: 12709594]
4. Byun J, Mueller DM, Fabjan JS, Heinecke JW. *FEBS Letters.* 1999; 455:243–246. [PubMed: 10437781]
5. Kirsch M, Korth H-G, Sustmann R, de Groot H. *Biol. Chem.* 2002; 383:389–399. [PubMed: 12033430]
6. Mondal B, Kumar P, Ghosh P, Kalita A. *Chem. Commun.* 2011; 47:2964–2966.
7. Hu X, Wang J, Zhu X, Dong D, Zhang X, Wu S, Duan C. *Chem. Commun.* 2011; 47:11507–11509.
8. Rosenthal J, Lippard SJ. *J. Am. Chem. Soc.* 2010; 132:5536–5537. [PubMed: 20355724]
9. Lim MH, Lippard SJ. *Acc. Chem. Res.* 2007; 40:41–51. [PubMed: 17226944]
10. Wang SH, Han MY, Huang DJ. *J. Am. Chem. Soc.* 2009; 131:11692–11694. [PubMed: 19645465]
11. Terai T, Urano Y, Izumi S, Kojima H, Nagano T. *Chem. Commun.* 2012; 48:2840–2842.
12. Kojima H, Nakatsubo N, Kikuchi K, Kawahara S, Kirino Y, Nagoshi H, Hirata Y, Nagano T. *Anal. Chem.* 1998; 70:2446. [PubMed: 9666719]
13. Chen Y, Guo W, Ye Z, Wang G, Yuan J. *Chem. Commun.* 2011; 47:6266–6268.
14. Yang Y, Seidlits SK, Adams MM, Lynch VM, Schmidt CE, Anslyn EV, Jason B, Shear J. B. J. *Am. Chem. Soc.* 2010; 132:13114–13116.
15. Hua Y, Sundar V, Christopher OO, Jay S, Rich GC. *Synthesis.* 2008; 6:957–961.
16. Yordanov ND, Iliev V, Shopov D. *Inorg. Chim. Acta.* 1982; 60:17–20.
17. Bitterwolf TE. *Inorg. Chim. Acta.* 2008; 361:1319–1326.
18. Gondal MA, Chang X, Al-Saadi AA, Zain H, Yamani ZH, Jun Zhang J, Ji G. *J. Environ. Sci. Health, Part A.* 2012; 47:1192–1200.
19. Goldstein S, Czapsk G. *J. Am. Chem. Soc.* 1995; 117:12078–12084.

20. <http://www.hse.gov.uk/coshh/basics/exposurelimits.htm>
21. Srinivas R, Samanta S, Chaudhuri A. Chem. Soc. Rev. 2009; 38:3326–3338. [PubMed: 20449052]
22. Chen WS, Yan WL, Huang L. Cancer Immunol. Immunother. 2008; 57:517–530. [PubMed: 17724588]

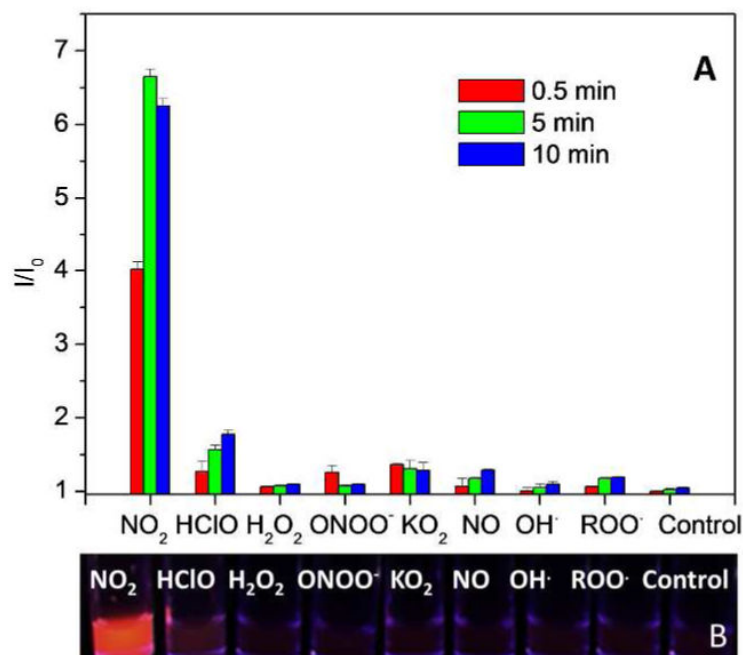


**Figure 1.**

*Ortho* isomer 6 is selective towards common ROS in physiological condition. (A) The graph was obtained by adding ROS (1  $\mu\text{M}$ ) into 6 (0.2  $\mu\text{M}$ ) delivered by 20 equivalent DOTAP in 10 mM PBS (pH = 7.4) at 37°C ( $\lambda_{\text{ex}} = 540 \text{ nm}$ ,  $\lambda_{\text{em}} = 590 \text{ nm}$ ). (B) Digital photos showing  $\text{NO}_2$ , not other ROS, turns on the fluorescence. Illumination of a 365 nm UV lamp at 5 min after adding ROS (5  $\mu\text{M}$ ) into 6 (1  $\mu\text{M}$ ) delivered by 20 equivalent DOTAP in 10 mM PBS (pH = 7.4).

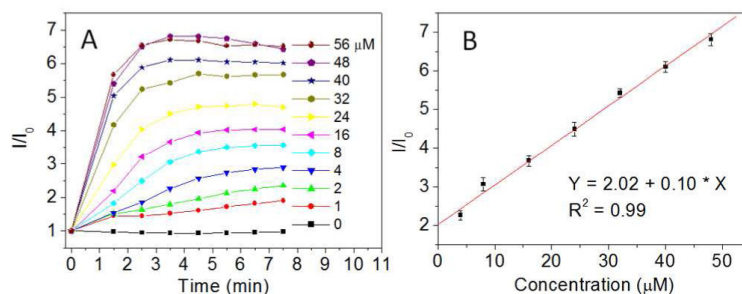


**Figure 2.**

Response of *ortho* isomer 6 to diethylamine NONOate at different concentrations in physiological conditions. (A) Increments of fluorescence intensity of 6 (0.2  $\mu\text{M}$ ) delivered by 20 equivalent DOTAP against time after the addition of diethylamine NONOate at different concentrations in 10 mM PBS (pH = 7.4) at 37°C ( $\lambda_{\text{ex}} = 540 \text{ nm}$ ,  $\lambda_{\text{em}} = 590 \text{ nm}$ ). (B) Dose response of the fluorescence intensity of 6 (0.2  $\mu\text{M}$ ) delivered by 20 equivalent DOTAP obtained 3.5 min after the addition of diethylamine NONOate in 10 mM PBS (pH = 7.4) at 37°C ( $\lambda_{\text{ex}} = 540 \text{ nm}$ ,  $\lambda_{\text{em}} = 590 \text{ nm}$ ).



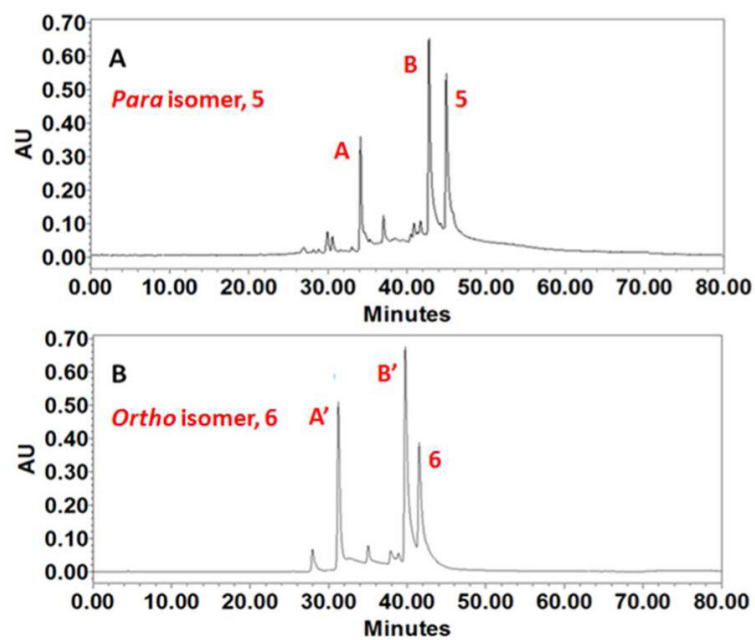


**Figure 3.** HPLC chromatograms of reaction products of 5 and 6 with nitrogen dioxide, recorded at 560 nm.

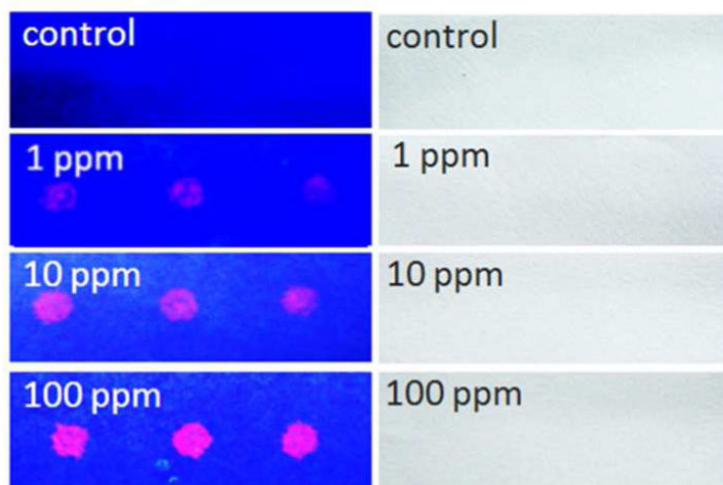


**Figure 4.** Visual detection of nitrogen dioxide gas. Nitrogen dioxide concentrations tested were 0, 1, 10, and 100 ppm respectively. Images on the left are taken under illumination of a 352 nm UV lamp (in the dark). For comparison, no color can be seen on images taken under laboratory lighting without UV light excitation.

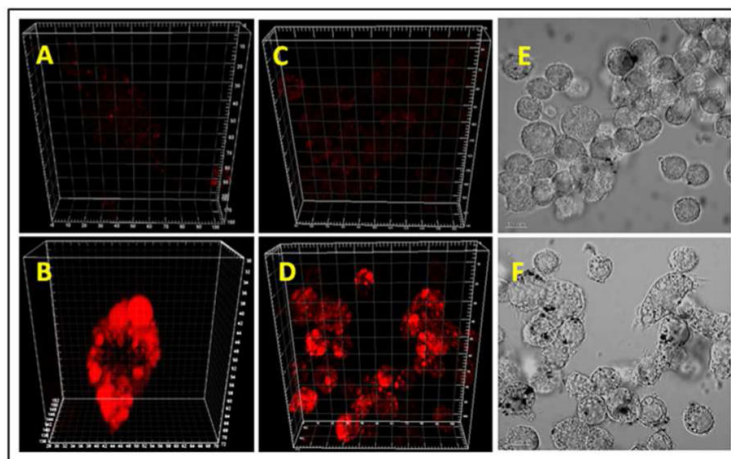
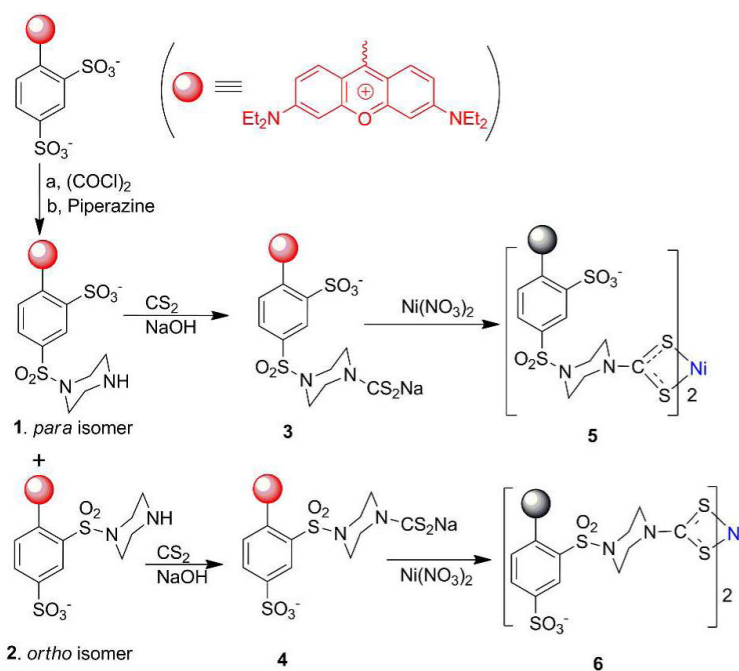
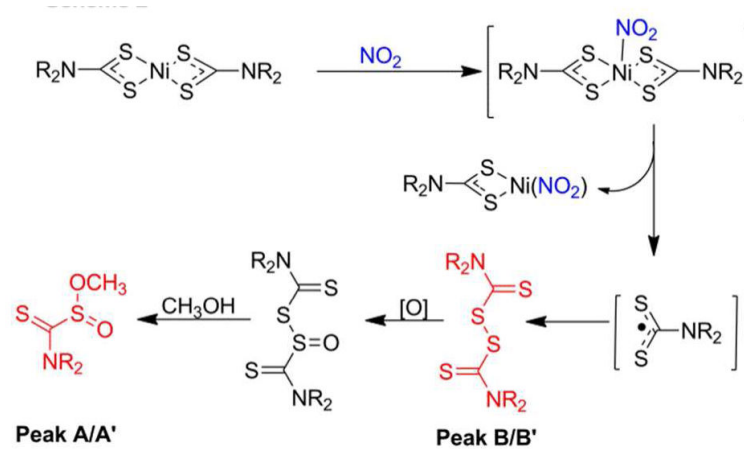


**Figure 5.**

$\text{NO}_2$  turns on the fluorescence of RAW 264.7 cells stained with 6. (A) and (B) are 3D images of single cell not treated and treated with DEANO (1 mM) respectively. (C) and (D) are 3D images of group of cells not treated and treated with DEANO (1 mM) respectively, together with their respective white field cell images (E) and (F).



Scheme 1.



Scheme 2.